

Velocity Measurements of a Jet Injected into a Supersonic Crossflow

Juan Gabriel Santiago* and J. Craig Dutton†

University of Illinois at Urbana–Champaign, Urbana, Illinois 61801

This paper presents a quantitative, experimental study of a single, sonic, underexpanded, transverse, round jet injected into a Mach 1.6 crossflow. This investigation is applicable to studies of supersonic combustors, thrust vector control of rocket nozzles, the cooling of nozzle walls, and jet reaction force prediction. Schlieren/shadowgraph photography and two-component, frequency preshifted laser Doppler velocimetry are used to visualize the flow and to measure three mean velocity components, five of the six kinematic Reynolds stresses, and turbulent kinetic energy at over 4000 locations throughout the flowfield. The study focuses on the transverse, midline plane and on two crossflow planes. These measurements are used to study the size and orientation of the recirculation regions upstream and downstream of the jet; the structure and strength of the bow shock, barrel shock, and Mach disk; the structure, strength, and development of the kidney-shaped, counter-rotating vortex pair; the growth of the annular shear layer between the jet plume and the crossflow; and the growth of the boundary layer beneath the jet. In addition, the present study provides validation data for analytical and numerical predictions of the transverse jet flowfield.

Introduction

RESURGENT interest in the development of supersonic combustors has motivated the study of transverse jet injection into a supersonic flow (TJISF). The need to inject, mix, and burn fuel quickly and efficiently is important because of the short residence times associated with supersonic combustors. The design of a supersonic combustor that uses TJISF as a means of fuel injection and mixing requires a fundamental understanding of these flows.

A schematic of a typical underexpanded TJISF flowfield is shown in Fig. 1. The plane shown in this figure is hereafter referred to as the midline, transverse plane of this flowfield. The figure shows the supersonic freestream flowing from left to right with the jet injected through the bottom wall. The obstruction caused by the jet generates a bow shock in the freestream. A small recirculation region near the surface is created just ahead of the jet. The internal structure of the jet itself is similar to that of a gaseous jet injected into a quiescent medium.¹ After leaving the orifice, the high-pressure, under-expanded jet expands through a Prandtl–Meyer fan centered at the nozzle lip before compressing through an interception shock structure (i.e., a barrel shock) and a Mach disk. As it passes through the Mach disk, the jet fluid loses much of its momentum and is then quickly turned downstream. Much of the jet fluid, however, passes through the oblique shocks that define the sides of the barrel shock. Downstream of the barrel shock structure, the jet cross section grows as it is further mixed into the crossflow. Immediately downstream of the jet and near the surface is another recirculation region. Downstream of the barrel shock, the velocity field of the jet plume is dominated by two streamwise-oriented, counter-rotating vortices that form a kidney shape in the crossflow planes and persist far downstream.

There have been numerous studies of the fluid mechanics of the TJISF flowfield. The impetus for such research has been the study of supersonic combustor fuel injection, thrust vector control of rocket nozzles, and jet reaction force prediction. As a result of these studies, the qualitative structure of the TJISF flowfield is fairly well understood. In addition, there have been a number of quantitative studies concerning the description of the TJISF flowfield structure and mixing characteristics.

Schetz and Billig² present a discussion of the effective back pressure, which is viewed as the pressure that determines the degree of expansion of the jet and is a function of the complex pressure field in the region near the exit of the jet. These authors also identified the jet-to-crossflow momentum flux ratio as the most important parameter that determines jet penetration. This ratio, J , may be written as

$$J \equiv \frac{\rho_j V_j^2}{\rho_c V_c^2} = \frac{\gamma_j P_j M_j^2}{\gamma_c P_c M_c^2} \quad (1)$$

where ρ , V , γ , P , and M are density, velocity, specific heat ratio, pressure, and Mach number, respectively, and the subscripts j and c indicate properties of the jet and crossflow. Billig et al.³ present a discussion of the analogy between the freejet and TJISF flowfields.

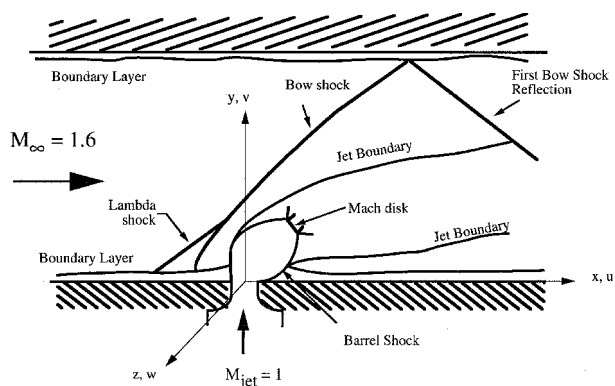


Fig. 1 Typical flowfield of a sonic, underexpanded transverse jet injected into a supersonic flow.

Received April 24, 1996; revision received Oct. 30, 1996; accepted for publication Nov. 6, 1996. Copyright © 1996 by the American Institute of Aeronautics and Astronautics, Inc. All rights reserved.

*Graduate Research Assistant, Department of Mechanical and Industrial Engineering; currently at The Aerospace Corporation, 2350 East El Segundo Boulevard, El Segundo, CA 90245-4691. Member AIAA.

†Professor, Department of Mechanical and Industrial Engineering, Associate Fellow AIAA.

There have been several three-dimensional numerical studies of circular jets injected into supersonic flows.⁴⁻⁶ All of the studies referred to here have solved the three-dimensional, compressible, Reynolds-averaged, Navier-Stokes equations using the Baldwin-Lomax turbulence model. Many of these studies show good comparison with experimental data. However, the results of these numerical studies were compared with only jet wall pressure and jet penetration data. Comparison with jet penetration and wall pressure does not ensure that a code correctly models jet spreading, jet mixing, turbulent kinetic energy production, or many other aspects of the velocity field.

There have also been numerous experimental studies of jets injected into crossflows. Margason⁷ presented an extensive review of experimental studies of, primarily, jets injected into subsonic crossflows. A notable study is that of Andreopoulos and Rodi⁸ who used three-sensor hot-wire anemometry to obtain three-component mean velocity measurements and all six Reynolds stresses. Another study, described in several reports,⁹⁻¹¹ presents detailed velocity measurements of the flow near the jet orifice and analyses of the development of the kidney-shaped, counter-rotating vortices of the plume.

Several experimental studies have also determined various aspects of the structure of jets injected into a supersonic flow.¹²⁻¹⁵ These descriptions of the structure include shock shape and location, jet concentration profiles throughout the flowfield, the geometry of the separation regions upstream and downstream of the jet, and the static pressure field near the jet orifice. Papamoschou et al.¹⁶ performed a parametric experimental study of TJISF penetration vs several relevant flow parameters. As expected, they found that jet penetration depends mainly on the jet-to-crossflow momentum flux ratio.

Recent studies have provided further descriptions of the structure of the TJISF flowfield using laser-based flow visualization and measurement techniques.¹⁷⁻²⁰ These studies used laser-induced fluorescence (LIF) and Mie scattering to study jet mixing and to visualize large-scale turbulent structures. The study of VanLerberghe et al.²⁰ was performed in the same experimental facility and presents a comparison of multiple planar laser-induced fluorescence (PLIF) images of TJISF at the same flow conditions as the present study. When such instantaneous images are superimposed, they show that the bow shock generated by the obstruction of the jet is steady (at least in this facility). However, superimposed images of the barrel shock region suggest that this flow structure contains regions of unsteadiness. The most apparent unsteady region is on the windward side of the barrel shock, which appears to be slightly flattened in some of the images.

There are a few studies that provide either quantitative or semiquantitative measurements of the velocity fields of under-expanded jets injected into a supersonic flow.²¹⁻²⁴ These studies used primarily either pointwise LIF or PLIF to make velocity, temperature, pressure, and concentration measurements. However, the velocity measurements of these studies are limited to time-averaged measurements of mean velocities and are not as accurate as the present laser Doppler velocimetry (LDV) study. To date, only one previous study is known that uses LDV as the primary diagnostic in the study of the mean and fluctuating velocity field of TJISF. Gallard et al.²⁵ investigated the effect of jet heating on jet spreading and on the turbulent velocity fields of the TJISF flowfield using three-component LDV measurements and temperature measurements using thermocouples. The measurements presented were obtained in four crossflow planes and suggested that the vorticity and turbulent kinetic energy of the jet increased with temperature.

Despite the previously mentioned investigations, it is clear that a dearth of nonintrusive, quantitative mean velocity and turbulence measurements exists in the TJISF flowfield. Such measurements will add to the fundamental understanding of the fluid dynamic mechanisms and mixing processes of this flow. The current investigation uses LDV measurements of the

mean and turbulent velocity fields to study the characteristics of a sonic, underexpanded transverse jet injected into a Mach 1.6 crossflow. The experiments described here provide all three mean velocity components U , V , and W , as well as five of the six Reynolds stresses $\langle u'^2 \rangle$, $\langle v'^2 \rangle$, $\langle w'^2 \rangle$, $\langle u'w' \rangle$, and $\langle u'v' \rangle$ (see Fig. 1). These measurements are taken in the x - y , midline plane and in two y - z , crossflow planes.

Experimental Facility

The experiments performed in this study use the air-delivery system of the Gas Dynamics Laboratory. This facility has two compressors arranged in parallel that provide a 115-m³ tank farm with about 1 kg/s of air at 862 kPa. The supersonic wind tunnel used here has a Mach 1.6 nozzle and is 76 mm wide over the entire length. The wind-tunnel test section is 36 mm high. Flow conditioning is accomplished just upstream of the wind-tunnel nozzle by means of a short length of honeycomb and two screens. The wind-tunnel test section provides optical access on all four sides of the test section through fused silica (top and bottom) and float glass (side) windows. The two side windows provide viewing areas 406 mm long by 33 mm high. The top window provides a viewing area 330 mm long by 33 mm wide. The bottom window provides the same viewing area as the top except for the area blocked off by the 17.5-mm-diam counterbore in which the transverse jet nozzle is inserted. The jet nozzle has been inserted directly into the counterbore in the bottom window to maximize optical access.

The exit diameter of the axisymmetric jet nozzle d is 4 mm. The contour of the nozzle consists of a one-quarter segment of a 3:5 (minor axis:major axis) ellipse such that the major axis of the elliptical segment is perpendicular to the jet nozzle flow direction. The air for the jet is provided by a regulated line running from the facility air supply to the jet nozzle.

LDV System

The two-component LDV system used for these measurements consists of the following six main components: 1) a 4-W, Cooper Lasersonics (Lexel) argon-ion laser, 2) two-component LDV optics, 3) a six-jet atomizer, 4) a digital burst correlator, 5) a 486 personal computer, and 6) a traverse table. The blue (488 nm) and green (514.5 nm) lines from the argon-ion laser were used for these measurements.

The LDV optics consist of a four-beam, two-component system and were arranged in four different optical setups. Table 1 summarizes the characteristics of the measurement volume (MV) for all four optical arrangements as well as the characteristics of the LDV system. Silicone oil droplets with a mean diameter of approximately 0.8 μm (Ref. 26) were injected into the wind tunnel and jet flows and served as seed particles for the LDV measurements. The LDV system uses a TSI Inc. model IFA 750 digital burst correlator signal processor to measure the Doppler frequencies with a 0.05% (percentage of reading) resolution. The traverse table is used to automatically move the transmitting and receiving optics along both directions (x - y) of the midline, transverse plane with a positioner accuracy of $\pm 25 \mu\text{m}$ per 25 mm of travel. A controller, which provides the positioner control signal, is given instructions via a serial port of the 486 personal computer.

An error analysis including the uncertainties associated with fringe spacing determination, measurement volume alignment, velocity biasing, fringe biasing, velocity gradient biasing, statistical uncertainty (finite ensemble size), and processor accuracy has been completed.²⁷ Reference 27 discusses each of these sources of error individually, presents the relevant calculations and models by which the uncertainties were estimated, and presents an estimation of the total uncertainty associated with the mean and fluctuating velocity measurements of each of the four optical arrangements. Furthermore, Ref. 27 presents contour plots of the total velocity measurement uncertainties throughout the transverse, midline plane. The typical uncertainty in the mean velocity measurements is about

Table 1 LDV system characteristics

Component	Description
Laser	4 W Cooper Lasersonics (Lexel) argon-ion laser
Beam lines	Blue, 488 nm and green, 514.5 nm
Bragg cell frequency shift	40 MHz
Beam expansion ratio	1.0
Transmitting lens	350-mm focal length
Beam spacing	13 mm
Fringe spacing	13.1 μm (blue), 13.9 μm (green)
Fringe velocity	524 m/s (blue), 556 m/s (green)
Number of fringes	12 (blue), 12 (green)
MV dimension in streamwise direction	Optical arrangements, nos. 1, 2, and 4: 0.17 mm Optical arrangement no. 3: 0.46 mm
MV dimension in transverse direction	Optical arrangements, nos. 1, 3, and 4: 0.17 mm Optical arrangement no. 2: 0.35 mm
MV dimension in spanwise dimension	Optical arrangements nos. 1 and 4: 0.35 mm Optical arrangement no. 2: 0.17 mm Optical arrangement no. 3: 0.5 mm
Collection lens	Optical arrangements nos. 1, 2, and 4: 120 mm focal length Optical arrangement no. 3: 250 mm focal length
Photomultiplier pinhole diameter	0.203 mm
Signal processor	TSI Inc. IFA 750 digital burst correlator
Seed particles	0.8- μm mean diameter silicone oil droplets

2% of U_c , where U_c is the velocity of the crossflow upstream of the leading bow shock. The typical uncertainty in the rms velocity fluctuation is about 3% of U_c . However, the uncertainty in the rms fluctuations may be as high as about 10% of U_c for a small region near the windward side of the barrel shock and near the wall where velocity gradient biasing contributes to most of the error. Note that these estimates of velocity measurement uncertainty do not include the effects of particle lag through strong shocks, estimates of which have been reported by Santiago.²⁷ However, this effect is discussed next.

Results and Discussion

During the experiments, the wind tunnel was run at its $M = 1.6$ design condition with a stagnation pressure of 241 kPa and a stagnation temperature of 295 K. These conditions yield a unit Reynolds number of $58.8 \times 10^6 \text{ m}^{-1}$. A sonic, underexpanded, transverse jet with a 4-mm exit diameter is injected into the test section through the bottom window. The jet conditions for the current study are the following: $P_{0j} = 476 \text{ kPa}$, $T_{0j} = 295 \text{ K}$, $J = 1.7$, and $Re_d = 1.11 \times 10^4$. These jet conditions provide a suitable jet penetration distance while achieving a sizable flowfield region around the jet orifice that is undisturbed by reflections of the bow shock from the top wall.

Schlieren/Shadowgraph Flow Visualizations

Schlieren and shadowgraph flow visualizations have been performed as a qualitative study of the TJISF flowfield. Visualizations were performed at several different jet-to-crossflow momentum flux ratios J to choose jet conditions suitable for the current study. Figure 2 shows a shadowgraph of the airjet case chosen for these experiments. The flow is from left to right and the jet is injected through the bottom wall at the location shown. Note that there exist at least seven jet diameters of undisturbed flow before the first bow shock reflection intersects the transverse jet flowfield.

Visible in the photograph is the Mach disk of the underexpanded sonic jet flow. Also, large-scale turbulent structures can be seen in the shadowgraph photograph, although their characteristics are difficult to discern because of the line-of-sight integrating nature of schlieren/shadowgraph photography. As in the previously discussed PLIF results of VanLerberghe et al.,²⁰ superimposed shadowgraph images taken at random times suggest that there is little or no bow shock movement, even in the area near the top wall where the bow shock is reflected.

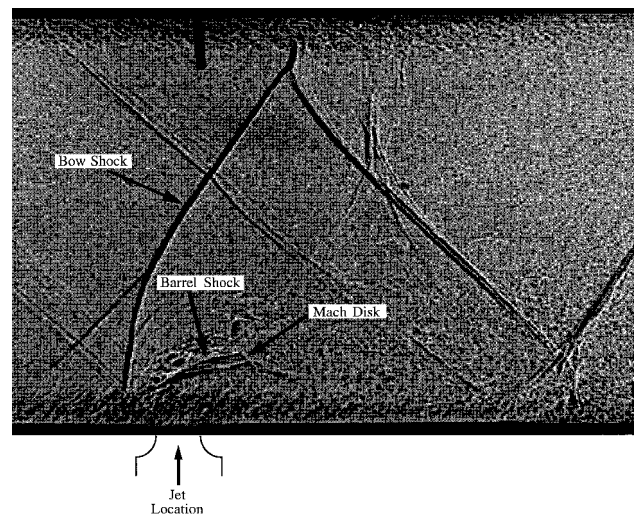


Fig. 2 Shadowgraph of the TJISF flowfield for the $J = 1.7$ airjet (flow is from left to right).

LDV Measurements

A number of characteristics of this TJISF flowfield make it a unique and challenging flow in which to obtain accurate velocity data. For example, the in-plane mean velocity vectors cover a range of angles of 360 deg and the velocity magnitudes range from zero to nearly 600 m/s. Also, the velocity gradients range from zero in the freestream to about 300 m/s/mm on the windward side of the emerging jet shear layer. The precise locations of the bow shock and its reflection, the separation shock, the barrel shock, and the Mach disk are, at first, all unknown. Finally, because the flow is highly three dimensional with the large gradients described earlier, effective measurement volume size and accurate measurement volume placement are both important issues.

Because of the complexities just described, the process of obtaining mean and turbulent velocity measurements involved several steps. The LDV measurement volume was located to within about $\pm 0.05 \text{ mm}$ in all three coordinate directions. Several LDV optical setups were used to determine the maximum, instantaneous particle velocity. Data on several increasingly fine grids were also obtained to locate high gradient regions. Bandpass filters of 40-MHz width were used throughout the flowfield. In many regions, the automated data acquisition sys-

tem needed to be paused between each spatial location to check the current velocity data histograms and update the input frequency filter settings of the signal processor. About five different input filter settings per channel were used in dozens of input filter setting combinations.

Velocity measurements were obtained at over 4000 spatial locations in the TJISF flowfield. Measurements at each of these locations were obtained at least twice using the four LDV optical arrangements described in Table 1. Over 4000 velocity realizations were obtained at each location to ensure statistical certainty.

Midline, Transverse Plane

Velocity measurements in the midline, transverse plane were obtained at over 2200 spatial locations. The majority of the measurements were made in the high-gradient near-jet region. This region extends from the bottom wall to a height of two jet diameters and from two diameters upstream to two diameters downstream. The maximum spacing between velocity measurement locations in the inner-jet region is 0.25 mm in the transverse y direction and 0.5 mm in the streamwise x direction. One-component LDV measurements near the wall (at $y = 0.5$ mm and below) were obtained only at locations upstream of $x/d = -0.5$ and downstream of $x/d = 0.5$ (i.e., on either side of the jet). The one-component setup is not capable of measuring the nearly vertically oriented velocities across the jet exit.

Approach Flow Measurements

The streamwise velocity component of the approaching freestream boundary layer was measured down to about $y = 0.25$ mm. Figure 3 is a plot of the boundary-layer velocity profile obtained five jet diameters upstream of the jet orifice center ($x = -20$ mm). The velocity measurements are shown together with a curve fit to the velocity profile given by Sun and Childs²⁸ for compressible, turbulent boundary layers. The integral thicknesses shown in the figure were determined using the ideal gas equation of state and the assumptions of negligible transverse pressure gradient, an adiabatic wall, and a recovery factor of 0.89 as suggested by Kays and Crawford.²⁹ The values for the shape factor H , wake strength parameter Π , skin friction coefficient C_f , and friction velocity u_τ , are also shown. The freestream Mach number along a traverse of the wind tunnel in the transverse direction was measured to be $1.59 \pm 1\%$ ($U_c = 446$ m/s).

Mean Velocity Measurements of Midline, Transverse Plane

Figure 4 shows a close-up of the mean velocity vector field in the inner jet region of the transverse, midline plane. Note that the velocity data in this region were obtained at more than twice the number of velocity vector locations presented. The

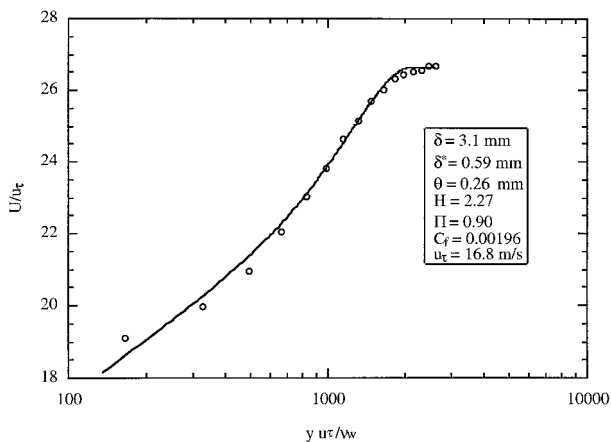


Fig. 3 Sun and Childs²⁸ curve fit of approaching boundary layer at $x/d = -5$.

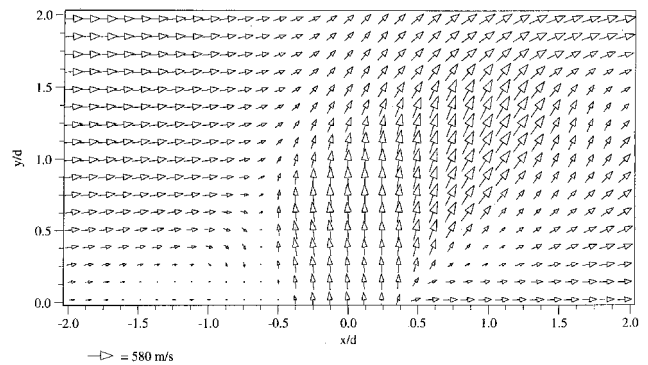


Fig. 4 Mean velocity vector field of inner jet region for midline, transverse plane.

experimental velocity vector data were placed on a uniform grid for the purposes of this figure. This was achieved by linear interpolation in both the x and y directions between the unequally spaced data. This interpolation routine preserved experimental data values that coincide with the locations shown. The crossflow direction is again from left to right with the 4-mm-diam jet injected from the bottom wall and centered at $x/d = 0$. In all succeeding figures (including all vector and contour plots), the coordinate system is centered on the jet as shown in Fig. 1.

Figure 4 shows the large gradients in the regions between the inner jet core and the crossflow. The velocity vectors clearly define the barrel shock region of the emerging jet core that is terminated by the Mach disk. Also shown are the low-velocity regions on the windward and leeward sides of the jet that are caused by the obstruction of the supersonic jet core. The flow approaching the jet from the left side (downstream of the normal section of the bow shock) is subsonic and the flow velocities outside of the boundary layer increase in the transverse direction because of the curvature of the bow shock. Also, the approaching boundary layer grows quickly as it nears the windward side of the jet. The region of adverse pressure gradient upstream of the jet and near the wall is similar to that just upstream of a cylinder in crossflow, except that in this case there is interaction between the jet and crossflow fluids. The approaching crossflow above about $y/d = 0.63$ is turned up with the jet and forms a three-dimensional shear-layer region between the jet and the crossflow. The approaching crossflow below about $y/d = 0.63$ is turned down toward the wall and there is a backflow region near the wall between about $x/d = -0.50$ and -1.50 . The flow approaching the jet stagnates near $x/d = -0.63$ and $y/d = 0.63$. This stagnation point lies between two regions of widely different velocity gradients. These regions are discussed further in the next section.

Everett et al.³⁰ and Santiago²⁷ discuss surface oil flow visualizations performed as part of the current study. These visualizations suggest that there are two reverse flow regions upstream of the jet and one reverse flow region downstream. However, although the two-dimensional velocity measurements were obtained within 0.19 jet diameters (0.75 mm) of the bottom wall, the present LDV measurements in the midline, transverse plane can adequately resolve only the recirculation region immediately upstream of the jet. The other two recirculation regions were too near the wall to be adequately resolved.

The recirculation region farthest upstream is probably a small, unsteady vortex that forms near the wall and just downstream of the separation caused by the bow shock/boundary-layer interaction. Next, the recirculation region immediately upstream of the jet corresponds to a horseshoe-shaped vortex that wraps around the windward side of the jet. The center of this recirculation region is at about $x/d = -1.25$ and $y/d = 0.13$. Lastly, the recirculation region downstream of the jet is smaller than that observed in the symmetry planes of trans-

verse jets injected into a subsonic flow.⁹ This difference suggests that the entrainment of crossflow fluid in this region is less for the TJISF than for a jet injected into a subsonic flow. In the present case, for transverse locations of about $y/d = 0.25$ – 0.75 , the region of the velocity field downstream of the leeward edge of the barrel shock accelerates rapidly as it moves downstream. This effect is most likely caused by crossflow fluid that has moved around the circumference of the barrel shock and impinges on itself on the midline plane.

The underexpanded jet flow is sonic at the orifice exit plane and accelerates to supersonic conditions in the vertical direction. The small boundary layer at the nozzle exit of the jet is seen in the bottom row of vectors just above the jet exit. As expected, the supersonic jet core flows vertically until it reaches a region (roughly one jet diameter from the orifice) where it is strongly influenced by the crossflow and is turned over as it accelerates toward the Mach disk. Note that the extent of the region of nearly vertical jet velocities (i.e., jet penetration) is a weak function of the boundary-layer thickness-to-jet diameter ratio, being larger for thicker boundary layers and vice versa.¹³

The maximum velocity immediately preceding the Mach disk is 589 m/s at about $x/d = 1.25$ and $y/d = 1.38$. Cohen et al.¹⁵ present a correlation based on an empirical fit of the experimental data of several authors (including that of Ref. 12) that can be used to calculate the height of the center of the Mach disk of a TJISF flowfield. Given the jet Mach number and jet-to-crossflow momentum flux ratio of the present study, the correlation of Cohen et al.¹⁵ predicts a Mach disk height of $y/d = 1.4$, which is in excellent agreement with the current study. The angle between this velocity vector and the streamwise direction is 55 deg. Assuming adiabatic flow in the inner jet core, this velocity corresponds to a maximum Mach number of 2.66 just before the Mach disk.

Although the flow deceleration through the Mach disk is clearly shown by the measurements in Fig. 4, particle lag effects through this strong normal shock result in an apparent deceleration region of about 1.5 mm length. Note, however, that much of the jet fluid does not pass through the Mach disk, but rather emerges from the barrel shock structure through the weaker oblique shocks that define its boundaries. The transverse, midline plane cuts this annular, supersonic shear-layer region in half. In Fig. 4, this three-dimensional region shows up as two regions of supersonic flow into which subsonic jet fluid that passed through the Mach disk is entrained. The jet fluid that passed through the Mach disk has little transverse momentum flux and is quickly turned downstream. This is shown in Fig. 4 by the small velocities downstream of the Mach disk (near $x/d = 1.75$ and $y/d = 1.5$). The greatest jet penetration is achieved by the supersonic flow that emerges from the windward side of the barrel shock and forms the supersonic mixing-layer region at the top edge of the jet trajectory.

Figures 5–7 show contour plots of the experimental measurements for the transverse, midline plane. The experimental data for all contours presented here were placed on a uniform grid by a linear interpolation kriging routine of Spyglass Transform software. The contour data were then smoothed to avoid high spatial frequency fluctuations that result from the interpolation. Also, note that some of the contours presented show significant streamwise gradients just above the jet orifice (within about $y = 0.75$ mm) and near the windward or leeward edges of the jet orifice. These gradients are a result of the interpolation described earlier.

Figure 5 shows contours of the mean Mach number field of the midline, transverse plane. The Mach number was determined from the velocity measurements by assuming that the flow is adiabatic (recall that the stagnation temperature of the jet and crossflow are equal). Once more, we see many of the features of the TJISF flowfield, including the change in Mach number through the leading bow shock, the rapid deceleration

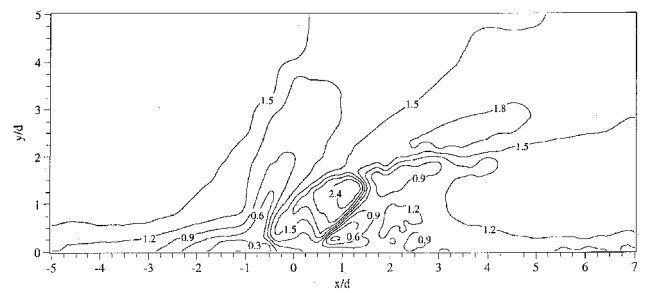


Fig. 5 Mean Mach number field of transverse, midline plane.

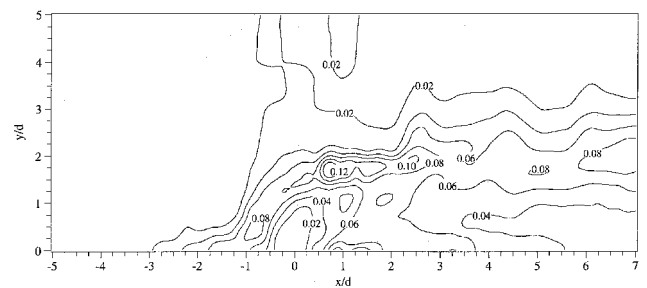


Fig. 6 Dimensionless TKE contours in transverse, midline plane.

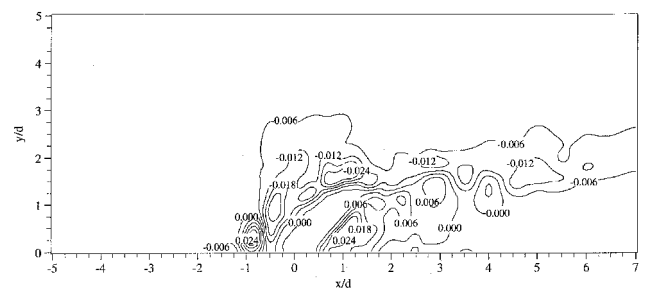


Fig. 7 Reynolds shear stress contours in transverse, midline plane ($\langle u'v' \rangle / U^2$).

of the crossflow as it approaches the jet, and the rapid acceleration downstream of the inner jet region. The acceleration inside the barrel shock region is clearly shown here, and the Mach disk location and orientation are also clear. Finally, note that the Mach number contours on the leeward side of the barrel shock are more closely spaced than those on the windward side. This may be caused by the slight unsteadiness of the windward side of the barrel shock region discussed earlier, which would act to smear the contours in this region. However, even the windward side has relatively closely spaced Mach number contours, which suggests that the effects of this unsteadiness are small.

Midline, Transverse Plane Turbulence Measurements

Contours of the turbulent kinetic energy (TKE) in the transverse, midline plane are shown in Fig. 6. The following, dimensionless form of TKE is used throughout this paper:

$$\text{TKE} = (\langle u'u' \rangle + \langle v'v' \rangle + \langle w'w' \rangle) / (2U^2) \quad (2)$$

where all three Reynolds normal stresses have been directly measured. Figure 6 shows the amplification of TKE in the region of the shock wave/boundary-layer interaction upstream of the jet. The high TKE regions in the shear layer between the inner jet region and the crossflow are also clearly seen. The inner jet itself, like the freestream, is predominantly inviscid and shows low TKE. Figure 6 also shows the regions of high TKE that lie just above and below the Mach disk in the shear layers on the windward and leeward sides of the barrel shock. The maximum measured nondimensional value

of TKE of about 0.12 occurs just downstream of the shear-layer region on the windward side of the barrel shock. Finally, note that after about three jet diameters downstream, the regions of high TKE are confined to transverse locations below about $y/d = 3.5$, and the contours don't seem to be spreading in the transverse direction quickly. This upper bound is indicative of the jet penetration.

Far downstream, the region of maximum TKE in the midline, transverse plane should yield a rough approximation of the jet centerline. A correlation presented by Orth and Funk³¹ for calculating the penetration of the jet centerline, defined as the location of maximum jet fluid concentration, in the transverse direction as a function of downstream distance, predicts transverse locations of $y/d = 2.1$ and 2.4 at $x/d = 5$ and 7 , respectively, for the current experimental conditions (see equation 5 of Ref. 31). In the present study, the corresponding values of the transverse location of maximum TKE are $y/d = 1.8$ and 2.1 , respectively.

Next, Fig. 7 presents a plot of the $\langle u'v' \rangle / U_c^2$ Reynolds shear-stress contours. The Reynolds stress is nondimensionalized here by the square of the approaching freestream velocity. Near the region of the stagnation point on the windward side of the barrel shock there are two regions of peak values of the $\langle u'v' \rangle / U_c^2$ Reynolds shear stress and these two regions are of opposite sign. These regions of high shear stress also correspond to regions of high mean velocity gradients. Therefore, large production of Reynolds shear stress and turbulent kinetic energy are expected to occur in these regions. The largest positive dimensionless shear-stress value of 0.08 occurs at about $x/d = -1.0$ and $y/d = 0.50$. The largest dimensionless negative shear stress of -0.056 occurs at $x/d = -0.50$ and $y/d = 1.25$.

Figure 7 also shows the large negative and smaller positive values of the $\langle u'v' \rangle / U_c^2$ Reynolds shear stress in the shear layers on the windward and leeward sides of the barrel shock, respectively. These two regions of opposite shear-stress sign exist throughout most of the jet trajectory. In fact, they are the most dominant feature of the $\langle u'v' \rangle / U_c^2$ shear-stress contours of the crossflow planes presented later. As the jet develops downstream, there is turbulent diffusion between these two regions and, far downstream, the $\langle u'v' \rangle / U_c^2$ Reynolds shear stresses are all negative. Also, the high gradient regions of the $\langle u'v' \rangle$ Reynolds shear-stress field across the jet cross section are diffused as the flow develops downstream. These trends are seen in the turbulence fields of jets injected into subsonic crossflows investigated by Andreopoulos and Rodi.⁸ Note that the region of relatively high $\langle u'v' \rangle / U_c^2$ Reynolds shear stress caused by the interaction of the jet and crossflow affects only a small part of the cross section of the midline plane for x locations downstream of about three jet diameters. For example, at $x/d = 7$ the $\langle u'v' \rangle / U_c^2$ Reynolds shear stress regions with magnitudes larger than 0.006 are less than a jet diameter wide in the transverse direction.

Finally, note that the $\langle u'w' \rangle / U_c^2$ and $\langle v'w' \rangle / U_c^2$ Reynolds shear stresses should be zero at the midline, transverse plane. In this plane of symmetry, the spanwise gradient of all quantities is negligible as well as the gradient and magnitude of the spanwise mean velocity. Andreopoulos and Rodi⁸ presented a discussion of the production mechanisms of the Reynolds shear stresses in the flowfield of a subsonic jet injected into a subsonic crossflow. Their discussion is also valid for the flowfield of the present study and is referred to later in this paper. Note that the values measured here for the $\langle u'w' \rangle / U_c^2$ Reynolds shear stress at the $z/d = 0$ centerline are 10–1000 times less than the corresponding peak values in the crossflow planes (see the next section).

Crossflow Planes

This section presents LDV measurements of the mean and turbulent velocity fields of the crossflow planes at $x/d = 3$ and 5 along with a discussion of these measurements. Measurements were obtained at about 821 locations for each of these

planes. The rectangular crossflow planes extend from the bottom wall to a height of four jet diameters above the wall and from the jet orifice midline to a spanwise distance of 3.75 diameters in the z direction. The maximum spacing between velocity measurement locations in the crossflow planes is 0.5 mm in the vertical direction. The spacing in the horizontal direction is 0.5 mm for $z/d = 0$ to 2.5 and 1.0 mm for greater values of z/d .

A series of spanwise traverses (in the z direction at fixed y) of the mean and fluctuating components of velocity was obtained throughout both sides of the z -symmetry plane to study the degree of symmetry in the crossflow planes. This symmetry study was carried out for both the $x/d = 3$ and 5 crossflow planes. These traverses extended from $z/d = -2$ to 2.25 and were located at $y/d = 1.0, 1.25, 1.50,$ and 2.0 . The LDV system could not be moved further than 8 mm in the negative z direction ($z/d = -2$) because of spatial constraints and the degree of optical access. This symmetry study showed that the mean flow quantities over most of the crossflow planes are very symmetric with near zero gradients of all mean velocities and near zero magnitudes of spanwise mean velocity at $z/d = 0$. Mean velocity values in the negative z region were within about $0.03U_c$ of the corresponding velocity values in the positive z region.

The turbulent quantities of the crossflow plane at $x/d = 5$ were also highly symmetric (corresponding fluctuating velocities on either side of $z/d = 0$ were within about $0.02U_c$). However, the turbulent quantities of the crossflow plane at $x/d = 3$ showed some asymmetry. For example, this asymmetry resulted in turbulence intensities of the $y/d = 2$ traverse, which were as much as $0.15U_c$ greater in the negative z region than corresponding intensities in the positive z region. On the other hand, in the $y/d = 1$ traverse, turbulence intensities in the negative z region were as much as $0.18U_c$ lower than corresponding intensities in the positive z region. That is, the turbulence intensities were disproportionately large toward the outer second and fourth quadrants of the y - z plane at $x/d = 3$. The reason for this asymmetry is not clear. However, the results of the asymmetry study, together with the measurements of the midline, transverse plane, suggest that asymmetry in this flowfield is a phenomenon limited to the inner jet region just downstream of the barrel shock structure.²⁷ Note also that a very similar asymmetry was found by Snyder and Orloff¹⁰ in LDV measurements of mean velocity in the flowfield of a subsonic jet injected into a subsonic crossflow.

Mean Velocity Measurements of Crossflow Planes

The in-plane components of the mean velocity vector field (V and W) of the crossflow planes at $x/d = 3$ and 5 are shown in Fig. 8 and are superimposed on contours of the mean streamwise velocity (U/U_c) field. The dominant flow feature is the large vortex that is one of the kidney-shaped, counter-rotating vortex pair described previously. At $x/d = 3$, the center of rotation of this vortex is near $y/d = 1$ and $z/d = 0.5$. With respect to the upstream crossflow plane, the center of rotation at $x/d = 5$ moves upward and outward to about $y/d = 1.38$ and $z/d = 0.63$. The maximum measured upwash, transverse velocity decreases only slightly from 207 to 194 m/s from the upstream to the downstream plane, and the location at which this velocity occurs moves along the centerline from $y/d = 1.38$ to 1.44 . These velocities are also the largest magnitude, in-plane velocities of the crossflow planes.

As in all the contours presented in this paper, the mean streamwise velocity contours of Fig. 8 show relatively small spanwise gradients near the symmetry plane. These contours also show the large gradients of the inner jet region. Unlike the flowfield of a subsonic jet in a crossflow,^{7–9} the present underexpanded jet compresses through a barrel shock and a Mach disk. Accordingly, the streamwise velocity measurements of the crossflow planes show local minima at the $z/d = 0$ centerline, which correspond to the jet core downstream of

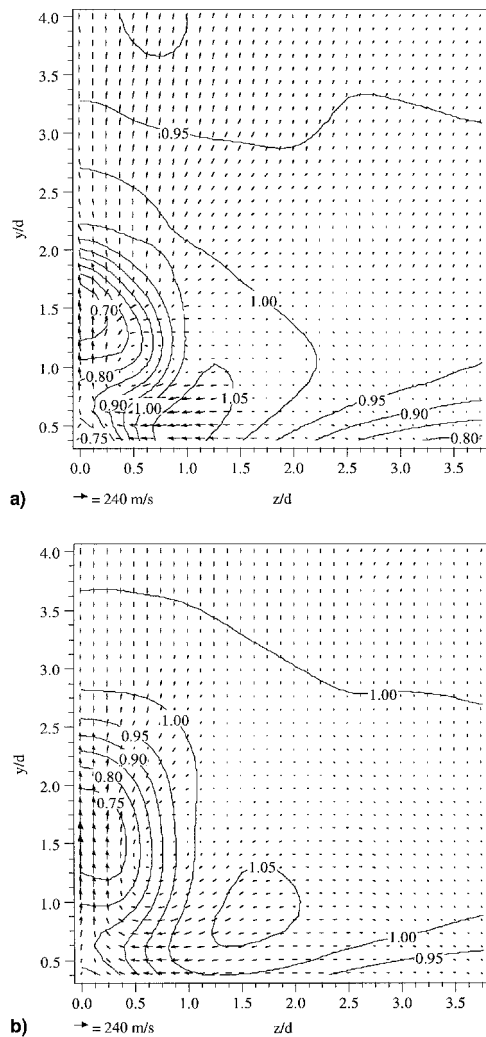


Fig. 8 V - W velocity vector field of crossflow planes. $x/d =$ a) 3 and b) 5.

the Mach disk. The gradients of streamwise velocity in this region are positive in a roughly radial direction from these minima. These gradients show the annular shear layer between the jet plume and the crossflow fluid. This shear layer is separated from the thick jet wall boundary layer by a region with relatively large streamwise velocities of about $U/U_c = 0.85$. Like the measurements in the inner jet region of the midline, transverse plane, this separation between the jet and boundary layer suggests that crossflow fluid has moved around the circumference of the barrel shock and impinges on itself in the midline, transverse plane. Figure 8 also shows the relatively slow-moving fluid of the thick boundary layer beneath the jet plume as well as the thick, nearly undisturbed boundary layer far from the $z/d = 0$ centerline.

Contours of the dimensionless mean streamwise vorticity field, $\zeta_x d/U_c$, where

$$\frac{\zeta_x}{U_c/d} = \frac{d}{U_c} \left(\frac{\partial W}{\partial y} - \frac{\partial V}{\partial z} \right) \quad (3)$$

are presented in Fig. 9 for the crossflow planes at $x/d = 3$ and 5. The vorticity of the counter-rotating vortex pair dominates the streamwise vorticity field of these planes. At $x/d = 3$, the maximum measured streamwise vorticity of $\zeta_x d/U_c = 0.64$ occurs at $z/d = 0.50$ and $y/d = 1.0$. On the other hand, at $x/d = 5$, the maximum measured streamwise vorticity is substantially reduced to $\zeta_x d/U_c = 0.42$ and occurs at $z/d = 0.38$ and $y = 1.25$. As expected, the locations of these maxima roughly co-

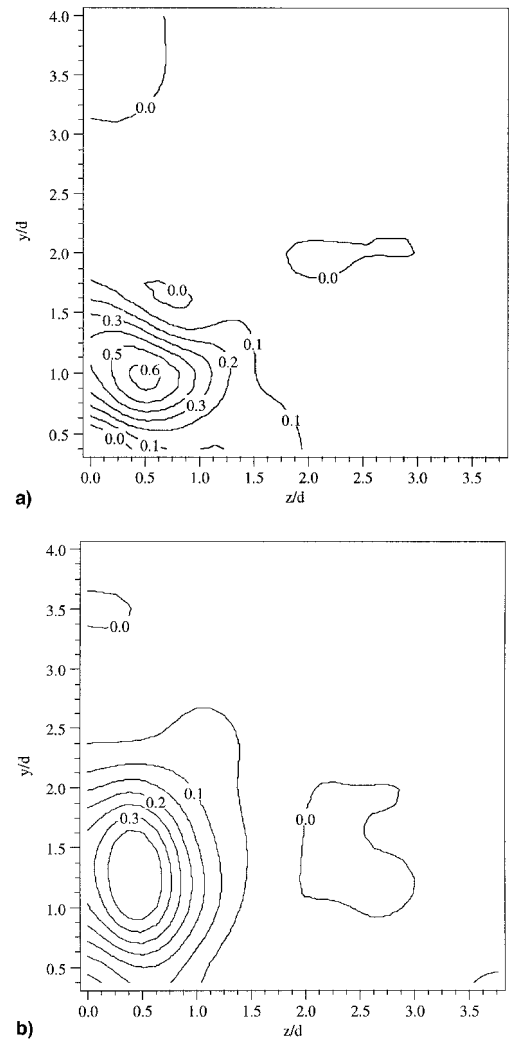


Fig. 9 Dimensionless mean flow streamwise vorticity ($\zeta_x d/U_c$) contours in crossflow planes. $x/d =$ a) 3 and b) 5.

incide with the center of rotation of the vortex (see Fig. 8). Also, note the difference in shape of the vorticity contours of the two crossflow planes. This difference is probably because, at the upstream plane, the motion of each vortex is constrained by the other vortex and by the wall.

Fearn and Weston³² give an equation for calculating the integrated strength Γ (i.e., the circulation) of each vortex as

$$\Gamma = \int_0^{2\pi} \int_0^{\infty} \zeta(r, \theta) r \, dr \, d\theta \quad (4)$$

where ζ is the mean flow vorticity and the origin of the polar coordinate r is at the center of the vortex. The integral is performed over the jet cross section, half-plane.²⁷ In the present study, the velocities at the center of rotation of the crossflow plane vortices have relatively small transverse components downstream of about $x/d = 3$; in this region, the velocity vector of the center of these vortices is less than 2 deg above the streamwise direction. Therefore, the jet cross sections at $x/d = 3$ and 5 can be approximated by these y - z crossflow planes. The integrated strengths of the crossflow plane vortices at $x/d = 3$ and 5 are 1.11 and 1.00 m^2/s , respectively. The decrease in strength is mainly because of the diffusion of vorticity across the symmetry plane.

Qualitatively, the structure of the vorticity contours presented here is very similar to those of Gallard et al.,²⁵ who presented the vorticity field of a crossflow plane at $x/d = 5$ for a TJISF with jet-to-crossflow momentum flux ratio of 10. This

similarity in structure includes the shape of the contours, the location of high-gradient regions, and the relative location of maximum vorticity with respect to the centerline.

Turbulence Measurements of Crossflow Planes

Contours of the TKE in the crossflow planes at $x/d = 3$ and 5 are presented in Fig. 10. These contours show the characteristic kidney shape as well as the high gradients of the jet plume. Even at $x/d = 3$, the pocket of low TKE fluid immediately downstream of the Mach disk that was apparent in the midline, transverse ($x-y$) plane has mostly been entrained into the highly turbulent fluid just downstream of the shear layer surrounding the barrel shock. Indeed, this entrainment and turbulence amplification may be enhanced by the oblique shocks near the triple points of the Mach disk. The shear-layer regions just above the jet core show high gradients of TKE. In addition, the TKE fields of the jet plume peak at a location away from the $z/d = 0$ midline and just below (i.e., in the negative transverse direction) the jet core. The maximum measured dimensionless TKE values of the jet plume were about 0.054 and 0.051 for the crossflow planes at $x/d = 3$ and 5, respectively. The TKE of the nearly undisturbed crossflow is less than about 0.005. Also, note that the region of high TKE in the jet plume grows faster in the transverse direction than in the spanwise direction as the jet develops. The extent of the region of large TKE in the transverse direction is probably a good measure of jet penetration and can be used to compare to the jet plume penetration correlation given by Papamoschou et al.¹⁶ Given the parameters of the current study, this corre-

lation predicts penetrations of $y/d = 2.4$ and 2.9 (defined as the penetration of the top part of the plume) for $x/d = 3$ and 5, respectively. This is in good agreement with the TKE measurements presented in Fig. 10, which show the top of the plume to be located at about $y/d = 2.3$ and 3.0 for $x/d = 3$ and 5, respectively.

Gallard et al.²⁵ presented the TKE contours of crossflow planes at $x/d = 5, 10, 15,$ and 17.5 for a TJISF flow with a jet-to-crossflow momentum flux ratio of 10. As in the case of the vorticity field, the structure of the TKE contours presented by these authors is very similar to those of the present study (note that these authors presented mainly vorticity, TKE, and temperature data). However, the data presented by these authors did not show the dramatic difference in the growth rates of the jet plume shear layer between the transverse and spanwise directions. This difference may be because the $J = 1.7$ jet plume of the current study is much more constrained by the jet wall upstream of about $x/d = 5$.

Figure 11 shows plots of the dimensionless $\langle u'v' \rangle / U_c^2$ Reynolds shear-stress contours in the crossflow planes at $x/d = 3$ and 5, respectively. At $x/d = 3$, the local minimum and maximum values are -0.014 (at $z/d = 0$ and $y/d = 1.89$) and 0.004 (at $z/d = 0.63$ and $y/d = 0.88$), respectively. At $x/d = 5$, the local minimum and maximum values are -0.013 (at $z/d = 0$ and $y/d = 2.38$) and 0.003 (at $z/d = 0.25$ and $y/d = 1.13$), respectively. That is, the local minima and maxima of $\langle u'v' \rangle / U_c^2$ for the two crossflow planes occur on the centerline at the top of the jet plume, and away from the centerline and below the jet plume, respectively. Also, as the jet plume separates

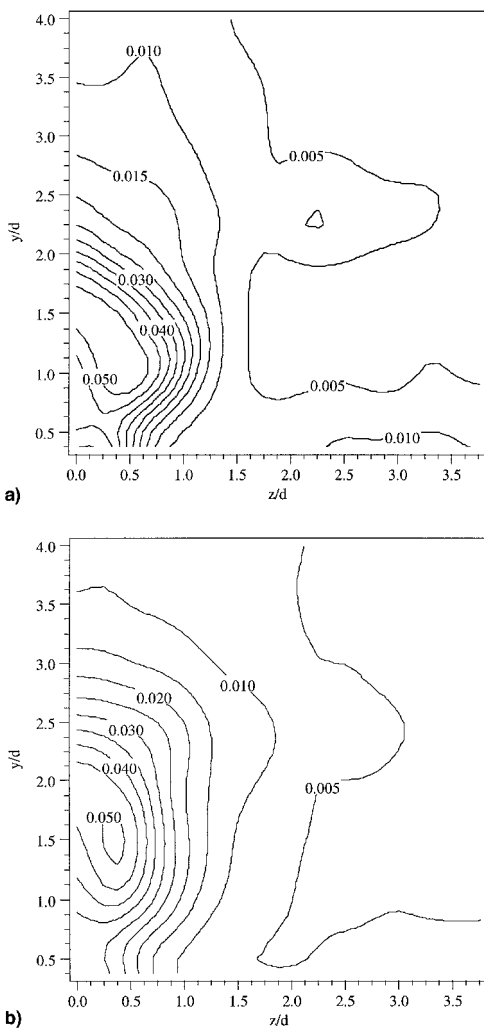


Fig. 10 Dimensionless turbulent kinetic energy contours in crossflow planes. $x/d =$ a) 3 and b) 5.

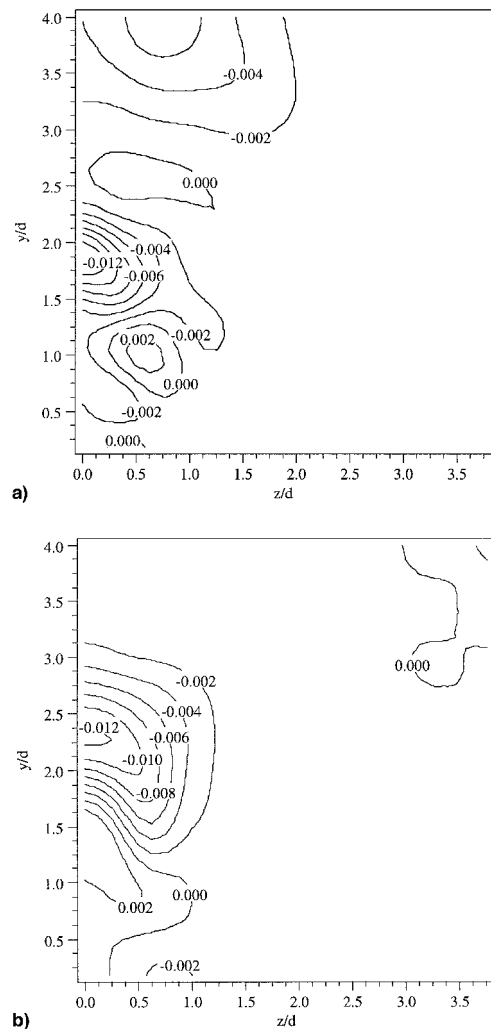


Fig. 11 $\langle u'v' \rangle / U_c^2$ Reynolds shear-stress contours in crossflow planes. $x/d =$ a) 3 and b) 5.

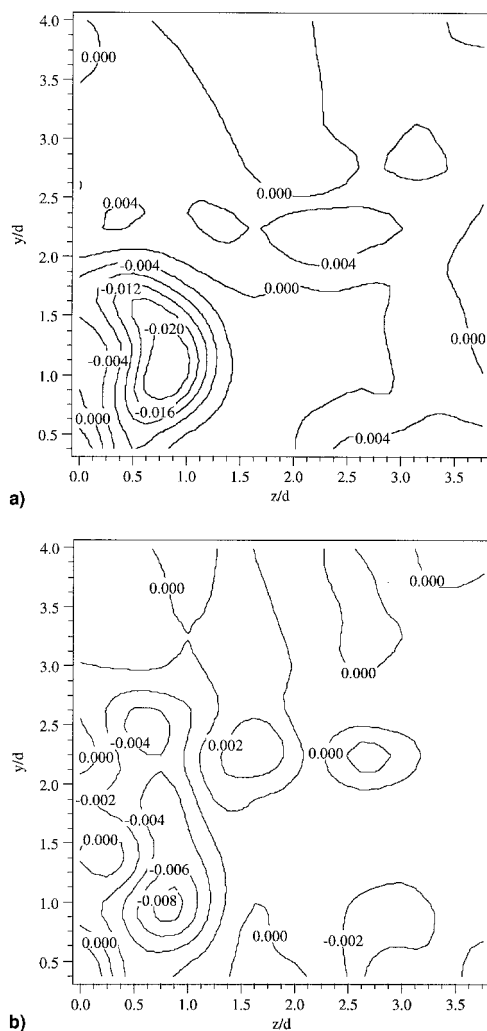


Fig. 12 $\langle u'w' \rangle$ Reynolds shear-stress contours in crossflow planes. $x/d =$ a) 3 and b) 5.

from the bottom wall, the local maximum moves toward the centerline. This is probably because, when the jet plume is near the bottom wall, the velocity gradients that generate the highest positive $\langle u'v' \rangle / U_c^2$ are found just off the midline. As the plume separates from the wall and the mean flow between the plume and the wall accelerates, the velocity gradients that generate the highest positive $\langle u'v' \rangle / U_c^2$ are found closer to the midline. This figure also clearly shows how the cross section of the jet plume increases in size and moves upward as the plume develops downstream.

Contours of the dimensionless $\langle u'w' \rangle / U_c^2$ Reynolds shear stress are given in Fig. 12 for the crossflow planes at $x/d = 3$ and 5. At $x/d = 3$, a minimum $\langle u'w' \rangle / U_c^2$ Reynolds shear-stress value of -0.024 occurs at $y/d = 1.0$ and $z/d = 0.75$. At $x/d = 5$, this local minimum has not moved very far with respect to the upstream crossflow plane (it is now at $y/d = 1$ and $z/d = 0.88$) and the magnitude has decreased to about 0.010. The region of negative shear stress near these local minima is the dominant feature of these contours. The three-dimensional boundary layer beneath the jet plume shows mostly positive, although small, values of this shear stress.

Measurements of the $\langle u'w' \rangle / U_c^2$ Reynolds shear stress reported by Andreopoulos and Rodi⁸ are similar to those of the current study. These authors present a discussion of the production mechanism of the $\langle u'w' \rangle / U_c^2$ Reynolds shear stress and suggest that, in the crossflow planes, the production of these stresses is mostly from the velocity gradients resulting from the vortex motion (particularly the $\partial W / \partial y$ gradients). In the present study, the $\partial W / \partial y$ gradient is largest within about a jet

diameter from the wall in a region between about $z/d = 0.13$ and 2.0. Also, the $\partial W / \partial y$ gradient is the largest gradient in the crossflow planes. Therefore, it is expected that a strong, negative $\langle u'w' \rangle / U_c^2$ stress should dominate in this region as shown in Fig. 12.

Summary and Conclusions

TJISF is a promising method of achieving the injection, mixing, and combustion of fuel in new supersonic combustion engines. Despite the numerous studies of this flowfield, there are significant gaps in the knowledge base. Most notable is the dearth of quantitative, nonintrusive measurements of the mean velocity and turbulence fields. The present investigation provides LDV measurements of the mean and turbulent velocity fields of a sonic, underexpanded transverse jet injected into a Mach 1.6 flow. The discussion presented earlier contained several conclusions concerning the TJISF flowfield. The following is a summary of these conclusions as well as observations and recommendations based on this study:

1) The observed recirculation region of the jet under study extends as far upstream as 1.5 jet diameters, and crossflow fluid as high as 0.5 jet diameters from the wall may be turned upstream. Because of this, it may be possible for jet fluid to exist anywhere within this upstream recirculation region and it is possible that this region could serve as an ignition zone in a reacting flowfield.

2) The fluid immediately downstream of the leeward side of the barrel shock accelerates rapidly in an area of low transverse velocity gradient. This, together with the fact that the Reynolds stresses in this area are relatively small, suggests that a stream of unmixed, crossflow fluid wraps around the circumference of the inner jet core and impinges on itself in the region between the wall and the jet plume. Because of fluid entrainment caused by the counter-rotating vortex pair, this is an important mechanism for mixing. Therefore, the designer of a supersonic combustor should carefully choose the spanwise separation of jets to take advantage of this effect. Also, this effect determines the strength of the jet's wake and may influence the spacing of injector holes in the streamwise direction.

3) The Mach number of the jet immediately preceding the Mach disk was measured to be 2.66, and the normal to the Mach disk surface was 55 deg above the streamwise direction. At the Mach disk, the jet loses much of its momentum flux and is quickly turned downstream.

4) The measured contours of Mach number suggest that the region of unsteadiness on the windward side of the barrel shock is small. Also, the recirculation region that is furthest upstream of the jet was too unsteady, small, and near the wall to be resolved. These issues are important not only because they affect the accuracy of the determination of shock location and the accuracy of the TKE measurements, but also because the designer of a supersonic combustor may wish to promote unsteadiness to enhance mixing.

5) The mean and fluctuating velocity fields of the crossflow planes show that the jet plume increases in size mostly in the transverse direction after about three jet diameters downstream of the orifice. This is probably a result of the motion of the kidney-shaped, counter-rotating vortices which, in the early stages of development, are severely constrained by the bottom wall at this momentum flux ratio. The manner in which a jet plume spreads is an important consideration in the determination of a supersonic combustor's configuration.

6) The motion of the kidney-shaped, counter-rotating vortices clearly dominates the velocity field of the jet plume far downstream. Also, the integrated strength of the counter-rotating, kidney-shaped vortices decreases by only about 9% from $x/d = 3-5$. Because the rate of decrease of the maximum upwash velocity is small as the flow develops downstream, the strength of these vortices is not expected to decrease rapidly.

7) The relatively large Reynolds shear stresses in the shear-layer regions of the flowfield suggest areas of highly correlated

(large-scale) turbulent structures. These regions are expected to have rapid mixing in a reacting flowfield.

8) The flow just downstream of the barrel shock is similar to the entrainment of a jet into a nearly parallel flow. In this region, an annular free shear layer forms between the jet plume and the crossflow. Also, the inner subsonic core of the jet is the relatively inviscid flow just downstream of the Mach disk, whereas the outer regions of the jet plume are the highly turbulent, supersonic fluid just downstream of the oblique shocks that define the barrel shock structure. As the flow develops downstream, the inviscid core is fully entrained into the turbulent regions of the jet plume and this entrainment may be enhanced by the oblique shocks near the triple points of the Mach disk. It may be advantageous to consider jet orifice configurations that promote turbulence and result in changes in jet cross section (e.g., a jet orifice with tabs) to enhance the entrainment described earlier and, presumably, promote overall mixing rates. Also, the size of the Mach disk relative to the cross section of the barrel shock is determined by the degree of underexpansion of the jet (see Adamson and Nicholls'). Therefore, the jet stagnation-to-effective back pressure ratio of TJISF may affect the entrainment of the inner jet core.

9) The stagnation point on the windward side of the barrel shock separates highly three-dimensional regions of widely different, large-magnitude velocity gradients. These small regions are also within a location of the flowfield that shows high TKE and a high $\langle u'v' \rangle$ Reynolds shear stress, both of which may be caused, in part, by the unsteadiness of the barrel shock structure. Therefore, numerical modeling efforts are advised to carefully consider the effects of grid size and turbulence models in these regions.

Acknowledgments

The authors acknowledge the support of the Rocketdyne Division of Rockwell International Corporation, under Contract R24QBZ92803049, with Munir M. Sindir as Monitor. In addition, the first author would like to acknowledge assistantship support from the University of Illinois SURGE and Alumni Teaching Fellow programs.

References

- ¹Adamson, T. C., Jr., and Nicholls, J. A., "On the Structure of Jets from Highly Underexpanded Nozzles into Still Air," *Journal of the Aerospace Sciences*, Vol. 26, No. 1, 1958, pp. 16–24.
- ²Schetz, J. A., and Billig, F. S., "Penetration of Gaseous Jets Injected into a Supersonic Stream," *Journal of Spacecraft and Rockets*, Vol. 3, No. 11, 1966, pp. 1658–1665.
- ³Billig, F. S., Orth, R. C., and Lasky, M., "A Unified Analysis of Gaseous Jet Penetration," *AIAA Journal*, Vol. 9, No. 6, 1971, pp. 1048–1058.
- ⁴Riggins, D. W., and McClinton, C. R., "A Computational Investigation of Mixing and Reacting Flows in Supersonic Combustors," AIAA Paper 92-0626, Jan. 1992.
- ⁵Clark, S. W., and Chan, S. C., "Numerical Investigation of a Transverse Jet for Supersonic Aerodynamic Control," AIAA Paper 92-0639, Jan. 1992.
- ⁶Aso, S., Tannou, M., Maekawa, S., Okuyama, S., Ando, Y., Yamane, Y., and Fukuda, M., "A Study on Mixing Phenomena in Three-Dimensional Supersonic Flow with Circular Injection," AIAA Paper 94-0707, Jan. 1994.
- ⁷Margason, R. J., "Fifty Years of Jet in Cross Flow Research," 72nd AGARD Fluid Dynamics Panel Meeting and Symposium on Computational and Experimental Assessment of Jets in Crossflow, Winchester, England, UK, April 1993.
- ⁸Andreopoulos, J., and Rodi, W., "Experimental Investigation of Jets in a Crossflow," *Journal of Fluid Mechanics*, Vol. 138, No. 1, 1984, pp. 93–127.
- ⁹Fearn, R. L., and Weston, R. P., "Induced Velocity Field of a Jet in a Crossflow," NASA TP-1087, May 1978.
- ¹⁰Snyder, P., and Orloff, K. L., "Three-Dimensional Laser Doppler Anemometer Measurements of a Jet in a Crossflow," NASA TM-85997, Sept. 1984.
- ¹¹Orloff, K. L., and Snyder, P. K., "Using a Three-Dimensional Laser Anemometer to Determine Mean Streamline Patterns in a Turbulent Flow," NASA TM-85948, July 1984.
- ¹²Zukoski, E. E., and Spaid, F. W., "Secondary Injection of Gases into a Supersonic Flow," *AIAA Journal*, Vol. 2, No. 10, 1964, pp. 1689–1696.
- ¹³Schetz, J. A., Hawkins, P. F., and Lehman, H., "Structure of Highly Underexpanded Transverse Jets in a Supersonic Stream," *AIAA Journal*, Vol. 5, No. 5, 1967, pp. 882–884.
- ¹⁴Schetz, J. A., Weinraub, R. A., and Mahaffey, R. E., Jr., "Supersonic Transverse Injection into a Supersonic Stream," *AIAA Journal*, Vol. 6, No. 5, 1968, pp. 933, 934.
- ¹⁵Cohen, L. C., Coulter, L. J., and Egan, W. J., Jr., "Penetration and Mixing of Multiple Gas Jets Subjected to a Cross Flow," *AIAA Journal*, Vol. 9, No. 4, 1971, pp. 718–724.
- ¹⁶Papamoschou, D., Hubbard, D. G., and Lin, M., "Observations of Supersonic Transverse Jets," AIAA Paper 91-1723, June 1991.
- ¹⁷McDaniel, J. C., and Graves, J., Jr., "Laser-Induced-Fluorescence Visualization of Transverse Gaseous Injection in a Nonreacting Supersonic Combustor," *Journal of Propulsion and Power*, Vol. 4, No. 6, 1988, pp. 591–597.
- ¹⁸Hermanson, J. C., and Winter, M., "Imaging of a Transverse, Sonic Jet in Supersonic Flow," AIAA Paper 91-2269, June 1991.
- ¹⁹Lee, M. P., McMillin, B. K., Palmer, J. L., and Hanson, R. K., "Planar Fluorescence Imaging of a Transverse Jet in a Supersonic Crossflow," *Journal of Propulsion and Power*, Vol. 8, No. 4, 1992, pp. 729–735.
- ²⁰VanLerberghe, W. M., Dutton, J. C., Lucht, R. P., and Yuen, L. S., "Penetration and Mixing Studies of a Sonic Transverse Jet Injected into a Mach 1.6 Crossflow," AIAA Paper 94-2246, June 1994.
- ²¹Fletcher, D. G., and McDaniel, J. C., "Laser-Induced Iodine Fluorescence Technique for Quantitative Measurement in a Nonreacting Supersonic Combustor," *AIAA Journal*, Vol. 27, No. 5, 1989, pp. 575–580.
- ²²Hollo, S. D., McDaniel, J. C., and Hartfield, R. J., Jr., "Characterization of Supersonic Mixing in a Nonreacting Mach 2 Combustor," AIAA Paper 92-0093, Jan. 1992.
- ²³Eklund, D. R., Fletcher, D. G., Hartfield, R. J., Jr., McDaniel, J. C., Northam, G. B., Dancy, C. L., and Wang, J. A., "Computational/Experimental Investigation of Staged Injection into a Mach 2 Flow," *AIAA Journal*, Vol. 32, No. 5, 1994, pp. 907–916.
- ²⁴Wang, K. C., Smith, O. I., and Karagozian, A. R., "In-Flight Imaging of Transverse Gas Jets Injected into Subsonic and Supersonic Crossflows," AIAA Paper 95-0516, Jan. 1995.
- ²⁵Gallard, R., Geffroy, P., Jacquin, L., and Losfeld, G., "Etude Experimentale Sur Les Interactions Entre Un Jet Supersonique Chauffe Transversal Et Un Ecoulement Supersonique Externe," AGARD Computational and Experimental Assessment of Jets in Crossflow, Winchester, England, UK, April 1993.
- ²⁶Bloomberg, J. E., "An Investigation of Particle Dynamics Effects Related to LDV Measurements in Compressible Flows," M.S. Thesis, Univ. of Illinois at Urbana-Champaign, IL, 1989.
- ²⁷Santiago, J. G., "An Experimental Study of the Velocity Field of a Transverse Jet Injected into a Supersonic Crossflow," Ph.D. Dissertation, Univ. of Illinois at Urbana-Champaign, IL, 1995.
- ²⁸Sun, C. C., and Childs, M. E., "A Modified Wall Wake Velocity Profile for Turbulent Compressible Boundary Layers," *Journal of Aircraft*, Vol. 10, No. 6, 1973, pp. 381–383.
- ²⁹Kays, W. M., and Crawford, M. E., "The Turbulent Boundary Layer for a Gas with Variable Properties," *Convective Heat and Mass Transfer*, 2nd ed., McGraw-Hill, New York, 1980, pp. 305–309.
- ³⁰Everett, D. E., Dutton, J. C., and Morris, M. J., "Pressure-Sensitive Paint Measurements of the Pressure Field About a Sonic Jet Injected Transversely into a Mach 1.6 Freestream," AIAA Paper 95-0524, Jan. 1995.
- ³¹Orth, R. C., and Funk, J. A., "An Experimental and Comparative Study of Jet Penetration in Supersonic Flow," *Journal of Spacecraft*, Vol. 4, No. 9, 1967, pp. 1236–1242.
- ³²Fearn, R. L., and Weston, R. P., "Vorticity Associated with a Jet in Cross Flow," *AIAA Journal*, Vol. 12, No. 12, 1974, pp. 1666–1671.